J. Fluid Mech. (1992), *vol.* 236, *pp.* 385–413
Printed in Great Britain

Subharmonic growth by parametric resonance

By M. R. HAJJ, R. W. MIKSAD AND E. J. POWERS
College of Engineering, The University of Texas at Austin, Austin, TX 78712, USA

(Received 29 November 1990 and in revised form 18 June 1991)

An experimental investigation is conducted in order to quantify the nonlinear and parametric resonance mechanisms that are associated with the subharmonic growth in the transition to turbulence in plane mixing layers. Higher-order digital statistical analysis techniques are used to investigate the nonlinear and parametric mechanisms responsible for the energy transfer to the subharmonic. The results show that the dominant interaction is a parametric resonance mechanism between the fundamental and the subharmonic modes which leads to a pronounced growth of the subharmonic. Measurements also indicate that the fundamental, besides interacting with the subharmonic, is also engaged in redistributing its energy to the other Fourier components of the flow via nonlinear three-wave interactions. Local wavenumber measurements verify that frequency–wavenumber resonance matching conditions exist between the fundamental and subharmonic in the region where the subharmonic gains its energy by parametric resonance. The results are in general agreement with theoretical models by Kelly (1967), and Monkewitz (1988) on subharmonic growth.

1. Introduction

Two important features of the transition to turbulence in plane mixing layers are the subharmonic growth and vortex pairing. The emergence and subsequent growth of a flow component at the subharmonic frequency, beyond the initial linear instability region, is a good example of secondary instability, and represents the first step in the sequence of instabilities that lead to the final breakdown to turbulence. Evidence of the growth of the subharmonic mode has been given in many experimental investigations, such as those of Sato (1959), Browand (1966), Miksad (1972) and many others. The mechanisms of vortex roll-up and subsequent pairing represent the vorticity restructuring in the transitioning mixing layer. Evidence of vortex pairing has been observed in the flow visualization pictures of Winant & Browand (1974) and Brown & Roshko (1974). Ho & Huang (1982) used hydrodynamic instability-wave concepts and flow visualization to compare the development of the fundamental and subharmonic modes to the vortex pairing mechanism in mixing layers. Their results showed that the saturation of the fundamental mode accompanies the vortex roll-up process, and that the saturation of the subharmonic mode accompanies the vortex merging. Also, the analysis of Pierrehumbert & Widnall (1982) showed that the emergence of a subharmonic component, in the two-dimensional case, may correspond to the pairing of two neighbouring vortices. Ho (1982) suggested a simplified model in which the mixing layer grows only by the vortex pairing mechanism. In general, the enhancement or suppression of the spreading mixing layer seems to be dependent on the ability to control this vorticity restructuring mechanism and consequently the subharmonic

growth. Although the initial development of the mixing layer can be satisfactorily described by spatial linear instability analysis, the relationship between subharmonic growth and the spectral energy exchanges which accompany vorticity restructuring of the transitioning mixing layer remains unknown. This relationship must be determined if we are to understand the mechanisms responsible for the subharmonic growth and if we are to determine the most effective way to control the spreading of mixing layers.

Kelly (1967) showed that the growth of the subharmonic mode in temporally developing mixing layers is most probably due to parametric resonance mechanism between a periodic component of the mean flow and the disturbances at the subharmonic frequency. The mean flow periodicity originates from a saturated finite-amplitude fundamental mode and is characterized by this mode's frequency and wavenumber. Monkewitz (1988) analysed the fundamental–subharmonic resonant interaction mechanism in a spatially growing mixing layer. The results indicated that a subharmonic mode evolving according to linear theory will be modified, on a slow space and/or time scale, by the presence of the fundamental mode. Monkewitz's spatial analysis, like Kelly's temporal analysis, assumes that the altered subharmonic does not affect the fundamental growth, which strongly suggests that a parametric mechanism is at work. One distinctive feature of the parametric mechanism is that a periodic component of the flow can serve as a means to extract energy from the mean flow and feed it to the subharmonic without sharing its own energy in the process. Also, parametric mechanisms lead to linear differential equations with periodic or quasi-periodic coefficients (Nayfeh 1987). In contrast, nonlinear resonance mechanisms, as defined by Raetz (1959), stem from nonlinear differential equations.

The analyses of Kelly (1967) and Monkewitz (1988) and their mathematical representation of the parametric resonance provide a conceptual and theoretical background for the parametric and nonlinear mechanisms associated with the subharmonic growth in plane mixing layers. However, experimental evidence and quantification of the parametric resonance mechanism are lacking. The spectral energy exchanges responsible for the subharmonic growth in the theoretical analyses of Kelly (1967) and Monkewitz (1988) remain unsubstantiated. Arguments based on the classical power spectra measurements provide no substantiative information on the efficiency and location of the nonlinear and parametric energy transfer to the subharmonic mode. Recent developments in digital polyspectral analysis for nonlinear systems now allow quantitative measurements of three-wave nonlinear couplings and spectral energy transfer. For example, Miksad *et al.* (1982) used complex demodulation and polyspectral analysis to identify the active nonlinear interactions in the transition of the wake of a flat plate. Ritz *et al.* (1988) used nonlinear quadratic transfer functions to measure the efficiency of the nonlinear interactions between the different modes in the transition to turbulence in a plane wake.

In this paper the frequency domain characteristics and the nonlinear energy transfer between the different modes in the transitioning mixing layer are investigated. Experimental evidence of the parametric resonance between the fundamental and subharmonic modes is presented. A quantification of the role of this mechanism in the subharmonic growth is established. This is done by measuring the linear and nonlinear energy transfer functions between the different components of the flow. Also, the spatial characteristics of the parametric resonance mechanism are discussed. The local phase speeds of the fundamental and its subharmonic are measured and experimental evidence for a resonance matching

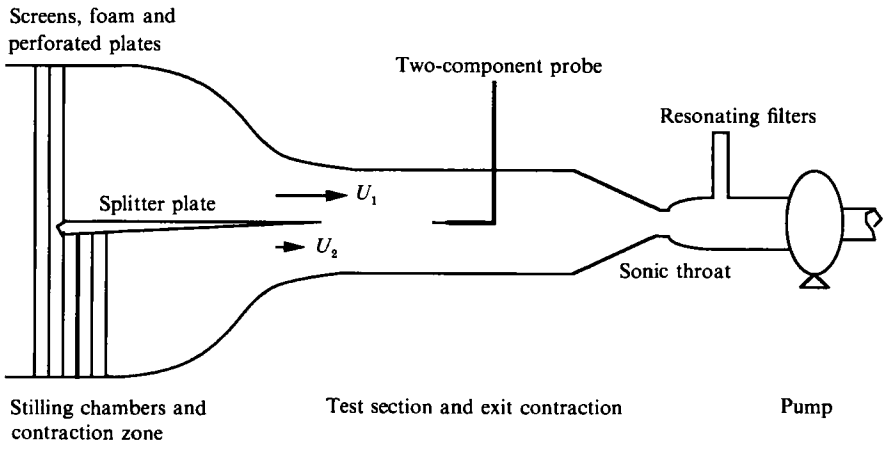

FIGURE 1. Schematic sketch of the wind tunnel apparatus.

condition in the wavenumber domain for efficient energy exchange via parametric resonance is established.

2. Experimental set-up

The experiments were conducted in a low-turbulence subsonic wind tunnel with a $30 \times 20 \times 150$ cm test section, see figure 1. The mixing layer was formed by merging two laminar streams as shown in figure 2. The upper and lower free-stream velocities were $U_1 = 7.17$ and $U_2 = 1.51$ m/s, respectively. This resulted in a velocity differential $\Delta U = 5.66$ m/s and a velocity ratio $R = (U_1 - U_2)/(U_1 + U_2) = 0.65$. The initial Reynolds number based on initial momentum thickness and upper free-stream velocity was 305. The free-stream turbulence intensity in the vicinity of the trailing edge of the splitter plate was $0.0005\Delta U$ in the high-speed stream, and $0.0011\Delta U$ in the low-speed stream. Most of the background turbulence was concentrated in frequencies below 40 Hz. Streamwise velocity fluctuations were measured using a DISA 56N/C hot-wire anemometry system. A special probe (Jones *et al.* 1988) with two sensing elements was used in these experiments to measure the spectral energy exchanges between two downstream locations, figure 2. The two sensing elements are separated in the streamwise direction by a distance $\Delta x = 0.1$ cm and in the spanwise direction by 0.15 cm, centre to centre. The cross-stream separation is zero. The small spanwise separation is used to isolate the downstream wire from the wake of the upstream wire. The hot-wire signals were DC and anti-alias filtered and were sampled with a CAMAC digital data acquisition system. The sampling frequency was set at 1000 Hz. The results shown here are for natural transition excited by random fluctuations in the flow. No external forcing was used. The measured frequency of the dominant instability mode of this transition was $f_0 = 215$ Hz.

3. Mean flow properties

The time-averaged flow properties were measured at midspan. The average velocity, $\bar{U} = \frac{1}{2}(U_1 + U_2)$ is equal to 4.34 m/s. The initial momentum thickness of the high-speed-side free-stream velocity, θ_0, is equal to 0.064 cm and the streamwise

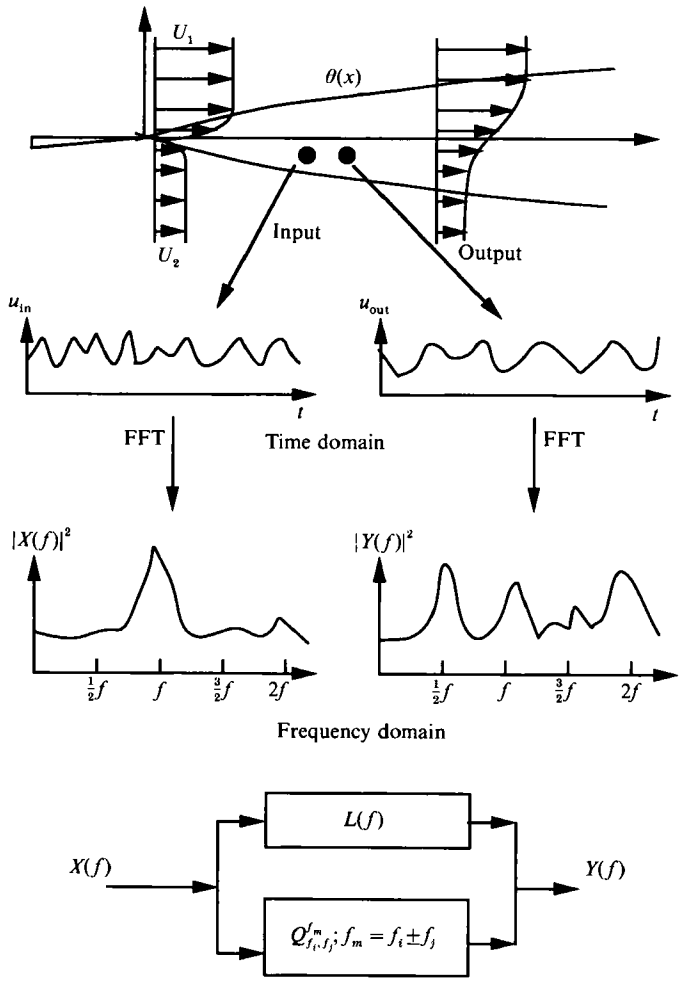

FIGURE 2. Schematic of the mixing layer and experimental approach.

wavelength of the dominant instability mode, λ_a, is equal to 1.98 cm. The Strouhal number of the dominant instability mode, $f_0\theta_0/\bar{U}$, is equal to 0.0317. In order to compare our results with data taken in experiments at different values of R, lengthscales are normalized with the ratio $R/\lambda_0 = 0.32$ as suggested by Huang & Ho (1990). The variations in the cross-stream direction of the longitudinal mean velocity and total r.m.s. fluctuations at different downstream locations are shown in figure 3. The mean velocity profiles are normalized according to the relation $2(U(y)-\bar{U})/\Delta U$. The velocity fluctuations are normalized with ΔU. The mean flow profiles show a combination of a wake and a mixing layer up to $Rx/\lambda_0 = 1.0$. Beyond this location, they become similar to a hyperbolic tangent profile.

The vertical spreading of the mixing layer is measured by the local momentum thickness, defined as

$$\theta = \frac{1}{\Delta U^2}\left\{\int_{-\infty}^{0} U(U-U_2)\,\mathrm{d}y + \int_{0}^{+\infty} U(U_1-U)\,\mathrm{d}y\right\}. \tag{1}$$

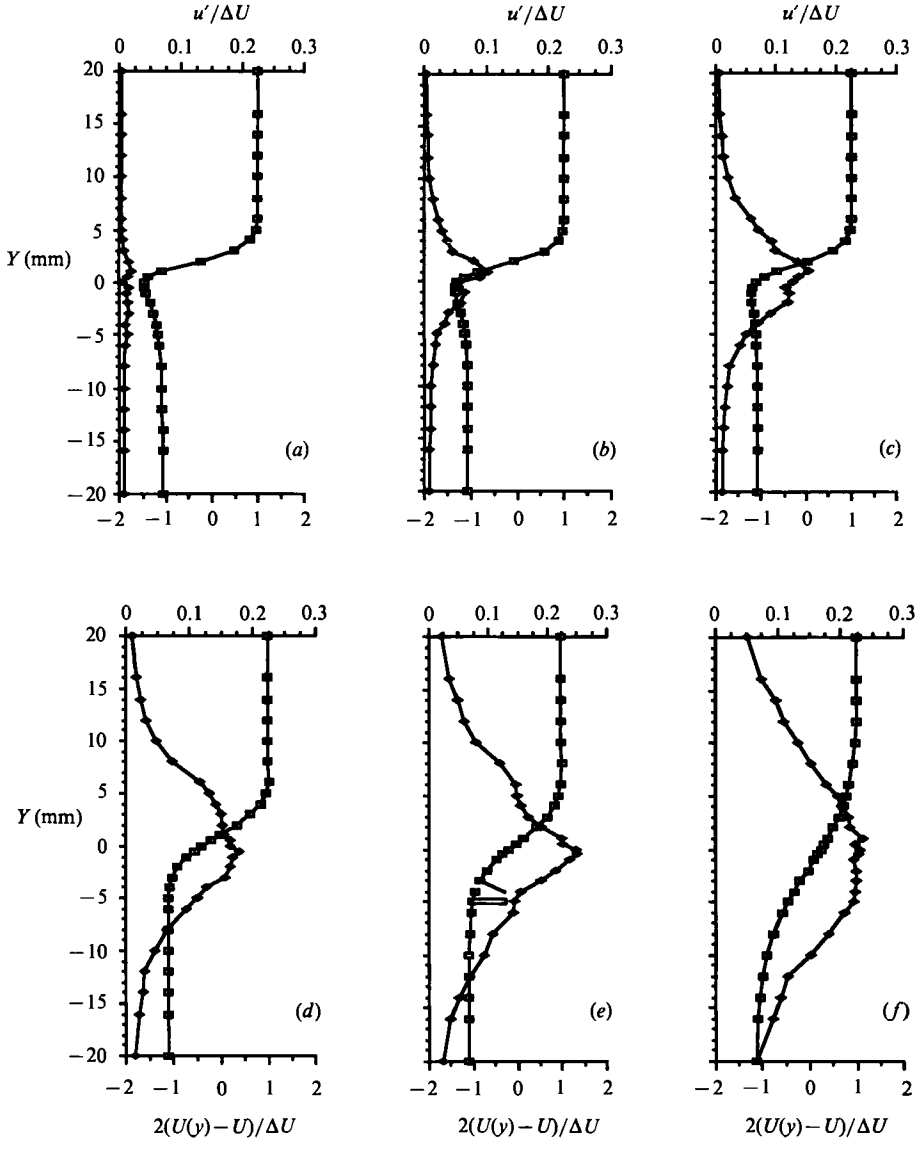

FIGURE 3. Cross-stream variations of the normalized mean velocity, $2(U(y)-U)/\Delta U$ (—⊡—), and longitudinal fluctuations, $u'/\Delta U$ (—◆—) at different downstream locations: (*a*) $Rx/\lambda_0 = 0.5$; (*b*) 1.0; (*c*) 1.5; (*d*) 2.0; (*e*) 2.7; (*f*) 5.0.

Similarly, an energy thickness, defined as

$$\epsilon = \frac{1}{\Delta U^3}\left\{\int_{-\infty}^{0} U(U^2-U_2^2)\,\mathrm{d}y + \int_{0}^{+\infty} U(U_1^2-U^2)\,\mathrm{d}y\right\} \tag{2}$$

is used as a measure of the flux of energy from the mean flow. The downstream development of the maximum u'_{rms} of the fundamental and subharmonic modes are shown in figure 4. The development of the energy thickness and the momentum thickness are shown in figure 5.

In figure 4, four basic regions of fundamental and subharmonic development are

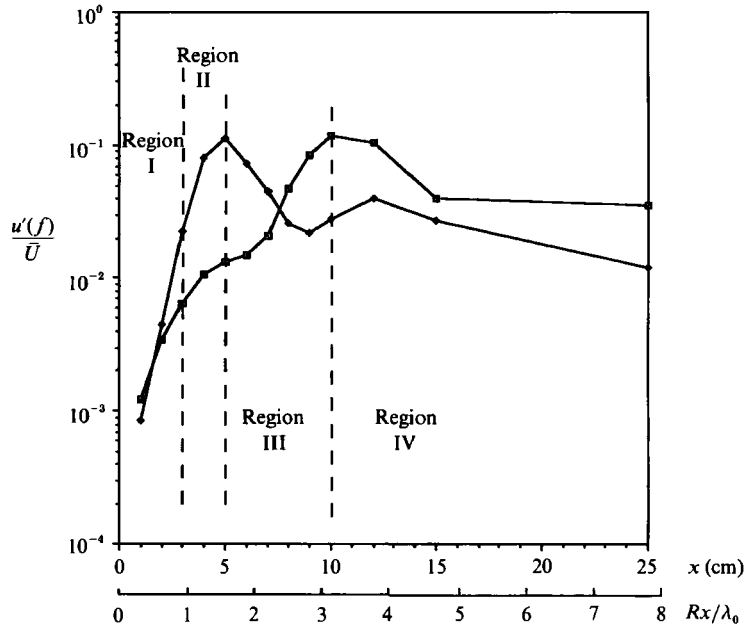

FIGURE 4. Variation of the r.m.s. amplitude of the fundamental (—⊡—) and subharmonic (—◆—) modes along max. u'_{rms} in the streamwise direction.

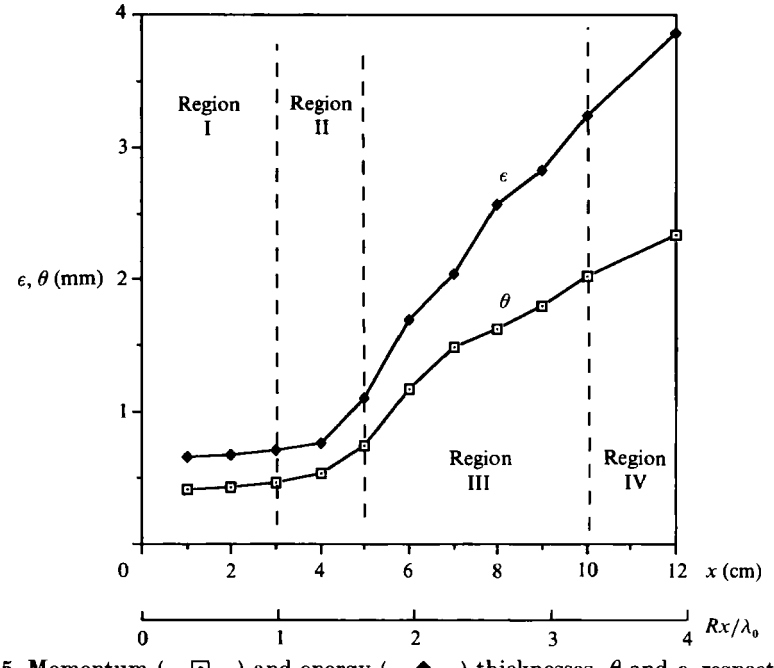

FIGURE 5. Momentum (—⊡—) and energy (—◆—) thicknesses, θ and ϵ, respectively, of the mixing layer *vs.* streamwise direction.

evident. For $Rx/\lambda_0 < 1.0$, the fundamental and subharmonic modes grow exponentially. The non-dimensional growth rate of the fundamental and the subharmonic, based on θ_0, are 0.10 and 0.047, respectively. These values are within 6% of the values predicted by the spatial linear instability analysis of Monkewitz &

Huerre (1982). The region limited by $Rx/\lambda_0 < 1.0$ represents the initial instability region where the fluctuations components grow exponentially, and will be referred to as Region I. At about $Rx/\lambda_0 = 1.0$, the subharmonic starts deviating from exponential growth. This location is chosen for reference because it is the last location at which the subharmonic amplitude deviates by less than 5% from the amplitude predicted by its initial exponential growth. Note that the choice of this criterion is subjective and is stated here for the sake of comparison. At this location, the r.m.s. amplitude of the longitudinal fluctuations at the fundamental frequency has an average value of $u'_{\rm rms}/\bar{U} = 0.012$ (peak value = 0.016). This value is almost twice the critical fundamental amplitude of $0.0153R^2 = 0.006$ predicted by Monkewitz (1988).

At $Rx/\lambda_0 = 1.6$, the fundamental achieves a saturation level of $0.113\bar{U}$. This level is one order of magnitude larger than that of the critical fundamental amplitude. Notice that up this location, figure 5 indicates that the vertical spreading of the mixing layer and the extraction of energy from the mean flow are very slow. The region between $Rx/\lambda_0 = 1.0$ and 1.6 represents a region where the fundamental mode continues to grow at a rate less than that predicted by the linear theory, to eventually equilibrate into finite-amplitude oscillations. This region will be referred to as Region II.

Between $Rx/\lambda_0 = 1.6$ and 3.2, the r.m.s. amplitude of the longitudinal fluctuations at the fundamental frequency decreases. However, the subharmonic component undergoes a second region of growth and achieves a saturation level of the same order of magnitude as the fundamental. The region limited by $Rx/\lambda_0 = 1.6$ and 3.2 will be referred to as the secondary instability region (Region III). In figure 5, we notice that a large spreading of the mixing layer also occurs over this region. The momentum thickness doubles between $Rx/\lambda_0 = 1.6$ and 3.2 indicating that the extraction of energy from the mean flow is increasing. If Kelly's (1967) interaction mechanism is correct, this implies that the energy is being extracted from the mean flow and transferred to the subharmonic by a parametric resonance mechanism. Beyond $Rx/\lambda_0 = 3.2$, the r.m.s. amplitudes of the longitudinal fluctuations at the fundamental and subharmonic modes start decreasing. This could be the result of the second subharmonic, $\frac{1}{4}f_0$, or the onset of the three-dimensional activities. This region will be referred to as Region IV.

4. Fundamental–subharmonic interaction

The primary aim of this investigation is to quantify the spectral energy exchanges arising from parametric or nonlinear wave–wave interactions that are responsible for the subharmonic growth in a plane mixing layer. These interactions can best be studied by using polyspectral analysis techniques. The role of these interactions in reinforcing the subharmonic can be quantified by measuring quantities such as the linear and nonlinear transfer functions. The connection between existing theoretical models of subharmonic growth and our use of the transfer function measurements is not obvious and the following heuristic model is presented to motivate this approach.

4.1. *Fundamental–subharmonic energy transfer*

As shown by many investigators and detailed by Mollo-Christensen (1971), the turbulent energy transfer from the mean flow to the primary instability components, and from the primary instability to the secondary instability components, and vice versa, occurs because of nonlinear terms that are present in the equations governing

energy exchange. The importance of these terms to the subharmonic generation process is evident in the equation governing energy exchanges between the different components of the velocity fluctuations, Stuart (1960). Monkewitz (1988), based on the experimental results of Ho & Huang (1982) and the discussion of Ho & Huerre (1984), assumed that subharmonic behaviour in mixing layers can be considered to be locally parallel in the saturation region of each mode in the subharmonic sequence. Kelly (1967) made a similar assumption in his temporal analysis. Following Monkewitz (1988) and Kelly (1967), the effect of interacting components on the growth of the subharmonic component in a parallel flow can be written as

$$\left\{\frac{\partial}{\partial t}\nabla^2+(U\nabla^2-U'')\frac{\partial}{\partial x}\right\}\psi(f_m)=\sum_{f_i\pm f_j=f_m}\sum\left\{-\left(\frac{\partial\psi(f_i)}{\partial y}\frac{\partial}{\partial x}-\frac{\partial\psi(f_i)}{\partial x}\frac{\partial}{\partial y}\right)\nabla^2\psi(f_j)\right.$$
$$\left.-\left(\frac{\partial\psi(f_j)}{\partial y}\frac{\partial}{\partial x}-\frac{\partial\psi(f_j)}{\partial x}\frac{\partial}{\partial y}\right)\nabla^2\psi(f_i)\right\},\quad f_m=f_i\pm f_j,\quad (3)$$

where $\psi(f_m)$ represents the subharmonic component of the stream function and $\psi(f_i)$ and $\psi(f_j)$ represent any two components whose interactions could lead to the subharmonic reinforcement. Note that the summation on the left-hand side is necessary to take into account all sum and difference interactions that could affect the subharmonic component.

The analyses of Kelly (1967) and Monkewitz (1988) showed that the manifestations of the parametric and nonlinear resonance mechanisms are different. In the nonlinear resonance mechanism, energy is passed to the subharmonic directly from the fundamental. In the parametric resonance mechanism, energy is not directly exchanged with the fundamental, but passed from the mean flow to the subharmonic as a result of the parametric variations introduced by the fundamental. These differences lead to different differential equations. While the nonlinear resonance mechanisms are modelled by nonlinear terms in the governing equations, the parametric resonance mechanism is a linear-like phenomenon in that it is modelled by linear terms with periodic coefficients resulting from the periodic distortions of the mean flow by the fundamental. It is important to note here that because coupling of the subharmonic with the fundamental mode is either directly or indirectly involved in both types of mechanisms, the phase coupling and wavenumber–frequency resonance conditions for the parametric interaction are similar to those required for nonlinear interactions.

Itoh (1977) showed that by decomposing the Fourier components of the stream function into a sum of linear eigenfunctions, (3) can be expressed as a wave coupling equation of the form

$$\frac{\mathrm{d}A(f_m)}{\mathrm{d}x}=\alpha(f_m)A(f_m)+\sum_{f_i\pm f_j=f_m}\sum\beta^{f_m}_{f_i,f_j}A(f_i)A(f_j),\quad f_m=f_i\pm f_j,\quad (4)$$

where $A(f)$ is the amplitude of the linear eigenfunction of the component with frequency f.

This coupling equation describes the spectral change of the complex amplitude of the frequency component f_m due to linear and quadratically nonlinear mechanisms. $\alpha(f_m)$ represents the linear growth, and $\beta^{f_m}_{f_i,f_j}$ is the nonlinear wave–wave coupling coefficient. The first step in determining these coefficients and hence the interaction physics, is to express (4) in terms of a transfer function equation that models these

physics. The coefficients of such an equation are then determined by measuring the changes in the complex amplitudes, $A(f)$, of the spectral component over a distance Δx. Equation (4) can then be transformed to an equation that relates the complex amplitude of the wave of frequency f_m at the downstream location, $x+\Delta x$, linearly to the complex amplitude of the same wave and quadratically to the complex amplitudes of all the interacting waves of frequencies f_i and f_j, that add or subtract to f_m, at the upstream location, x, see figure 2. Such a relationship is established by expressing (4) as

$$Y(f_m) = L(f_m)\,X(f_m) + \sum_{f_i \pm f_j = f_m} \sum Q^{f_m}_{f_i;f_j} X(f_i)\,X(f_j), \quad f_m = f_i \pm f_j. \tag{5}$$

In this equation, $Y(f_m)$ and $X(f_m)$ are the complex Fourier amplitudes at frequency f_m of the fluctuations at two points in space in the transitioning mixing layer, see figure 2. The quantities $L(f_m)$ and $Q^{f_m}_{f_i;f_j}$ are the linear and quadratic elements of the transfer function model, respectively, and are generally complex quantities. It is important to note here some of the characteristics of these transfer functions. First, the quadratic transfer function, unlike the linear transfer function, is a dimensional quantity. Second, the complex amplitude at the output frequency component is dependent on the product of the transfer functions and the complex amplitudes at the input frequencies. Third, the parametric reinforcement of f_m will manifest itself as a part of the dynamics represented by the linear portion of the transfer function since, as Nayfeh (1987) notes, the parametric approach to the fundamental–subharmonic interaction leads to linear equations with periodic or quasi-periodic coefficients. The subharmonic problem can thus be reduced to a simple transfer function system that is characterized by a parallel combination of linear and quadratically nonlinear transfer functions (see figure 2). Methods to estimate the linear and quadratic transfer functions are given by Kim & Powers (1988) and Ritz & Powers (1986).

4.2. *Wavenumber domain matching*

Instability-wave theory of parallel shear flows models the velocity fluctuations as travelling waves whose amplitudes may vary in time and space. The growth of these components can be affected by the linear instability mechanisms and by parametric and nonlinear interactions of the different components. Cross-bispectral analysis and transfer function modelling can be used to study the characteristics of the energy transfer due to these interactions between the different modes in the frequency domain. The spatial characteristics and wavenumber–frequency matching conditions between interacting waves play a particularly important role in this process. Bretherton (1964), for example, studied wave triad resonance and amplitude growth in a homogeneous medium. For a one-dimensional nonlinear equation, he showed that wavenumber resonance as well as frequency resonance is important for two modes to interact quadratically to drive a third mode. In the case of mixing layers, Monkewitz (1988) set the condition that the fundamental and subharmonic modes should travel at the same phase speed for an efficient transfer of energy to occur. Basically, this requires wavenumber as well as frequency resonance between the two modes. This condition was also assumed in the parametric resonance model of Kelly (1967).

Different methods of extracting spatial characteristics from time series data have been applied by many investigators. Stegen & Van Atta (1970) used the signals from two points separated in space to measure phase speeds of the Fourier components in

grid turbulence. Beall, Kim & Powers (1982) devised a technique to compute the local energy spectrum as a function of frequency and wavenumber, from simultaneous measurements of the time series at two points in space. From such a spectrum, one can then compute the dispersion relationship and the power spectrum in the wavenumber domain. In the case of transitioning flows, the measurement of the phase difference between fluctuations at two points may be random, which results in turbulent broadening of the dispersion relation. Thus, the wavenumber value as a function of time can be treated as a random variable with a probability distribution about a mean for each frequency mode. Wavenumber measurements in the present experiments were made using a two-tensor probe as described by Jones *et al.* (1988) and the technique devised by Beall *et al.* (1982). Notice that the separation between the two sensors should be sufficiently small compared to a wavelength and coherence length to avoid spatial aliasing and phase incoherence, respectively. For a defined wavenumber, we have

$$\left.\begin{aligned} X(f) &= A(f)_x \exp\{\mathrm{i}(k(f)_x + \phi(f)\}, \\ Y(f) &= A(f)_{x+\Delta x} \exp\{\mathrm{i}(k(f)_{x+\Delta x} + \phi(f))\}. \end{aligned}\right\} \tag{6}$$

Since $X(f)$ and $Y(f)$ are measured simultaneously, the phase $\phi(f)$ at both points is the same. The sample cross-power spectrum is then

$$X^*(f)\,Y(f) = A^*(f)_x A(f)_{x+\Delta x} \exp\{\mathrm{i}(k(f)\,\Delta x)\}. \tag{7}$$

The sample local wavenumber can then be related to the local phase of the sample cross-power spectrum and is given by

$$k(f) = \text{phase}\{X^*(f)\,Y(f)\}/\Delta x. \tag{8}$$

The computational technique for the wavenumber–frequency spectrum, $S(k,f)$, the wavenumber spectrum $S(k)$ and the dispersion relationship are given by Beall *et al.* (1982). In this investigation, this technique is used to study the spatial characteristics of the transition to turbulence in plane mixing layers and in particular the parametric resonance mechanism that results in the growth of the subharmonic.

5. Results and discussion

The results presented in this paper are based on measurements of the streamwise velocity fluctuations at cross-stream locations corresponding to the maximum of the u'_{rms} fluctuations. Miksad (1972) presented a detailed evolution of the u'_{rms} profiles for the various instability modes involved in the transition process. Estimates of the growth rates of the subharmonic and fundamental modes by Miksad (1972) based on maximum u'_{rms} differ only slightly (10% or less) from those determined by cross-stream integration of total u'_{rms}. Measurements made at the maximum u'_{rms} avoid problems of riding up or down a modal profile slope, a problem encountered when measurements are made at a constant cross-stream distance. Jones (1983) showed that the cross-stream location of maximum u'_{rms} also closely coincides with the cross-stream location of maximum u^3_{rms}, which, according to bispectral analysis marks the location where maximum nonlinear or parametric coupling occurs between interacting modes.

The variations of the power spectrum of the streamwise fluctuations in the downstream direction, along maximum u'_{rms}, are shown in figure 6. In Region I, at $Rx/\lambda_0 = 1.0$, the spectrum exhibits peaks at the fundamental frequency, $f_0 =$ 215 Hz, and its subharmonic, $\frac{1}{2}f_0$. The large energy content at the subharmonic mode

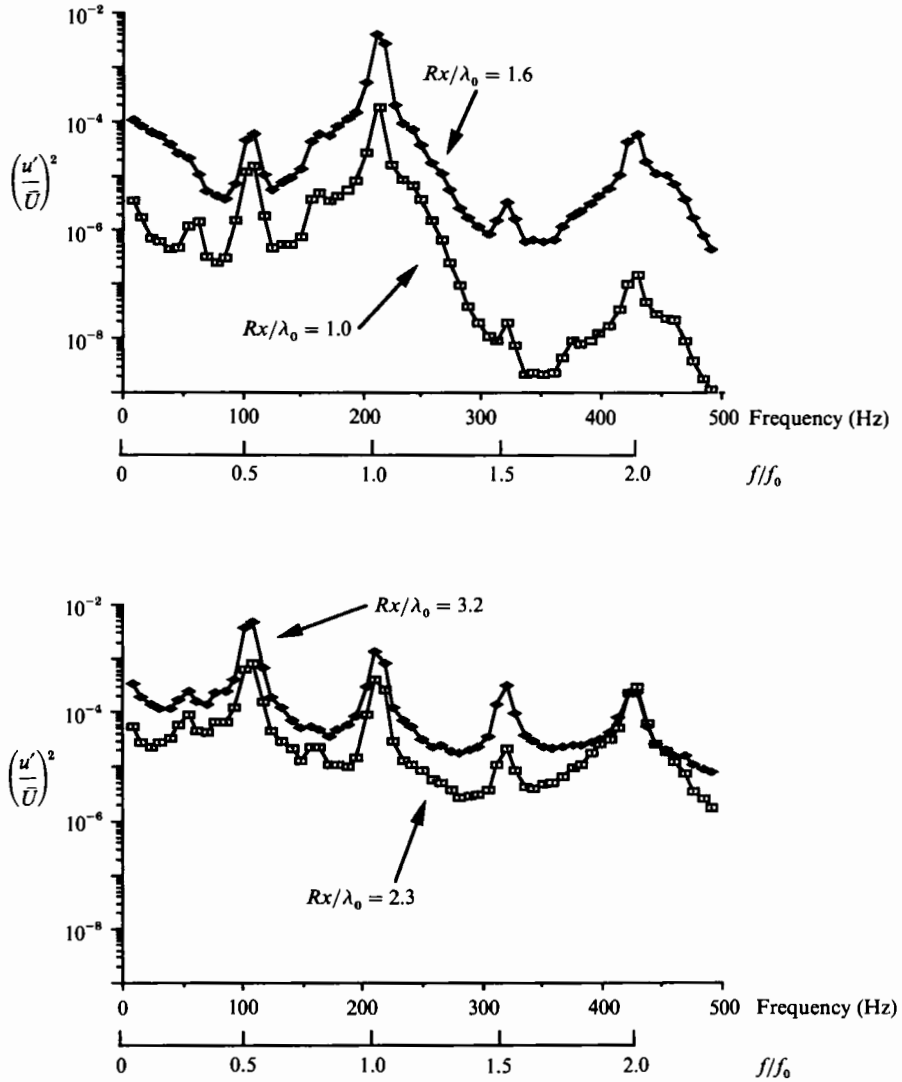

FIGURE 6. Variations of the power spectrum of the streamwise fluctuations in the downstream direction.

is due to the feedback of energy at this frequency from the vortex pairing mechanism. By $Rx/\lambda_0 = 1.6$ (i.e. Region II), both the fundamental and subharmonic modes have gained energy. Also, the band of fluctuations centred at $2f_0$ have gained a considerable amount of energy. The low-frequency components have also gained some energy. By $Rx/\lambda_0 = 2.3$ (i.e. Region III), the fundamental has lost some energy. However, the subharmonic continues to grow and the valleys between these modes and the other harmonics are filling rapidly.

The downstream development of the longitudinal fluctuations at the fundamental and subharmonic frequencies are shown in figure 4. Ho & Huang (1982) showed that the saturation of the fundamental corresponds to the vortex roll-up location, and the saturation of the subharmonic corresponds to the vortex merging location. In their experiment, the vortex roll-up occurred at $Rx/\lambda_0 = 2$ and the vortex merging at $Rx/\lambda_0 = 4$. In the present experiments, see figure 4, the fundamental and

subharmonic saturations occur at $Rx/\lambda_0 = 1.6$ and 3.2, respectively. The basic states of growth, equilibration and decay of the energy of the longitudinal fluctuations at the subharmonic and fundamental modes are observed and agree with the earlier results of Miksad (1972) and Ho & Huang (1982).

5.1. *Detection of coupled modes*

As the instability modes interact, they become coupled. The characteristics of energy transfers between coupled mode components cannot be determined by linear analysis. For example, the coherency function for a linear system, defined as

$$\gamma^2(f) = E[|X(f)\,Y(f)|^2]/\{E[|X(f)|^2]\,E[|Y(f)|^2]\},$$

where $E[\ldots]$ denotes an expected value, can only describe the linear relationship between the input $X(f)$ and the output $Y(f)$ at that same frequency. It cannot describe the interaction of two different frequency components, $X(f_i)$ and $X(f_j)$ at the input, to reinforce a third frequency component $Y(f_m)$ at the output, such that $f_m = f_i \pm f_j$. As noted by Powers & Miksad (1987), three-wave interactions can only be described by higher-order statistical moments, such as the cross-bispectrum.

The cross-bispectrum, defined as

$$B(f_i, f_j) = E[Y(f_m)\,X^*(f_i)\,X^*(f_j)],$$

where $f_m = f_i \pm f_j$ is a measure of the statistical dependence between the output spectral component at frequency f_m, $Y(f_m)$, and the input spectral components at frequencies f_i and f_j, $X(f_i)$ and $X(f_j)$, where $f_m = f_i \pm f_j$. The cross-bispectrum can only be non-zero if the frequency modes at f_i, f_j, and f_m are statistically dependent. In the case of three-wave interaction phenomena, this statistical dependence arises because of the phase coherence between the interacting waves. Thus, the product of the complex amplitudes of the three components will have a non-zero average over many realizations. The information that can be provided by the cross-bispectrum for the problem of subharmonic growth is of particular interest because it provides a means for detecting the presence of coupling between the fundamental and its subharmonic. A quantitative measure of this coupling is given by the cross-bicoherence squared

$$b^2(f_i, f_j) = |B(f_i, f_j)|^2/\{E[|X(f_i)\,X(f_j)|^2]\,E[|Y(f_m)|^2]\}.$$

It is important to note that the estimation of cross-bicoherence depends significantly on the number of realizations used to form an average. Figure 7, for example, shows that for one realization the cross-bicoherence will measure perfect coupling between the three modes under consideration. This is because in this case there is no averaging and the numerator and denominator are equal. As the number of realizations is increased, the level of bicoherence becomes lower. Finally, it converges to a constant value of 0.6 after 256 realizations. The results presented here show cross-bicoherence averaged over 256 realizations, each realization consisting of 128 samples.

Plots of the cross-bicoherence, along maximum $u'_{\rm rms}$, at different downstream locations are shown in figure 8. These locations were chosen to represent the different regions of growth of the fundamental and subharmonic modes. The values measured at $Rx/\lambda_0 = 0.32$ fall in the primary instability region or Region I. Values at $Rx/\lambda_0 = 1.6$ fall in Region II where the fundamental starts to saturate and the subharmonic has deviated from its exponential growth. Values shown for $Rx/\lambda_0 = 1.9$ and 2.3 fall in the secondary instability region or Region III. The results show that in

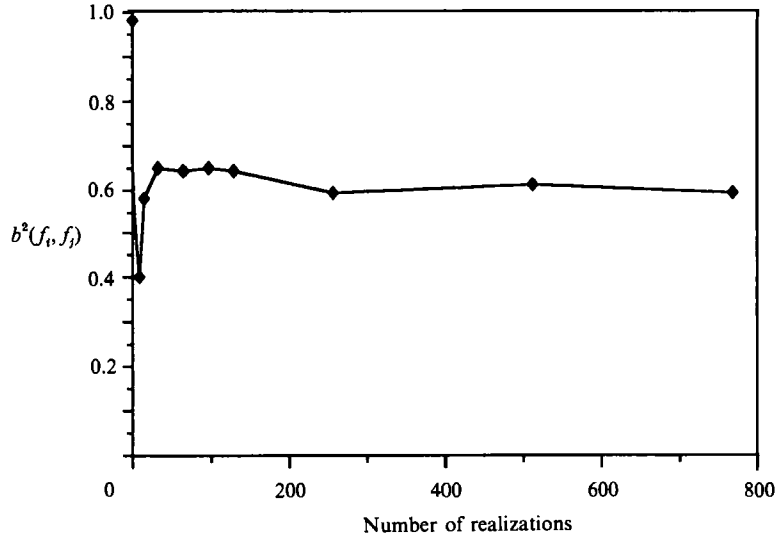

FIGURE 7. Convergence of the cross-bicoherence, $b^2(f_i, f_j)$, of a coherent frequency triplet as a function of the number of realizations.

region I, at $Rx/\lambda_0 = 0.32$, the strongest peak occurs at $(f_0, -\frac{1}{2}f_0)$. This shows that the fundamental mode and its subharmonic are phase coherent. This early phase coherence is the result of the feedback of energy from the downstream position where the subharmonic is emerging (vortex pairing is occurring), as suggested by Corke (1987). Although the phase coherency implies the possibility of nonlinear or parametric interaction and transfer of energy, we are still in the region of exponential growth where both modes are still growing at the linear rate predicted by the linear instability theory. The nonlinear effects are still minimal.

In Region II, at $Rx/\lambda_0 = 1.6$, the highest level of bicoherence appears at (f_0, f_0) and $(2f_0, -f_0)$ which indicates the production of the second harmonic via the self-interaction of the fundamental mode, as evidenced from the power spectra. Also, a new bicoherence pattern emerges where the contour level bands extend, away from (f_0, f_0) and $(2f_0, -f_0)$, to include fluctuations at $(f_0, f_0 - \delta f)$ and $(f_0 + \delta f, f_0)$ in the sum region and $(2f_0 \pm \delta f, -f_0)$ and $(2f_0 \pm \delta f, -f_0 \pm \delta f)$ in the difference region. These sideband bicoherencies indicate that the fundamental is coupling with fluctuations in its skirts to broaden the second harmonic. Note also the bicoherency between the fundamental and the subharmonic, $(f_0, \pm\frac{1}{2}f_0)$, and the fundamental and the $\frac{3}{2}$ harmonic, $(f_0, \pm\frac{3}{2}f_0)$. However, it is important to note that the level of bicoherence between the fundamental and its subharmonic, $(f_0, -\frac{1}{2}f_0)$, is lower in this region than in Region I. Note also that figure 4 shows that, in Region II, the subharmonic has deviated from exponential growth and started to equilibrate. Therefore, it appears that this equilibration of the subharmonic is accompanied by a reduction in the phase coherence between itself and the fundamental.

At the beginning of Region III, $Rx/\lambda_0 = 1.9$, where the subharmonic starts its second region of growth, the bicoherence level at $(f_0, -\frac{1}{2}f_0)$ is larger than that in Region II. This indicates that the growth of the subharmonic, in Region III, is accompanied by an increase in the level of its phase coupling with the fundamental. The above bispectral results demonstrate that the fundamental and subharmonic modes are phase-coupled over Regions I, II, and III of the transition. In Region I,

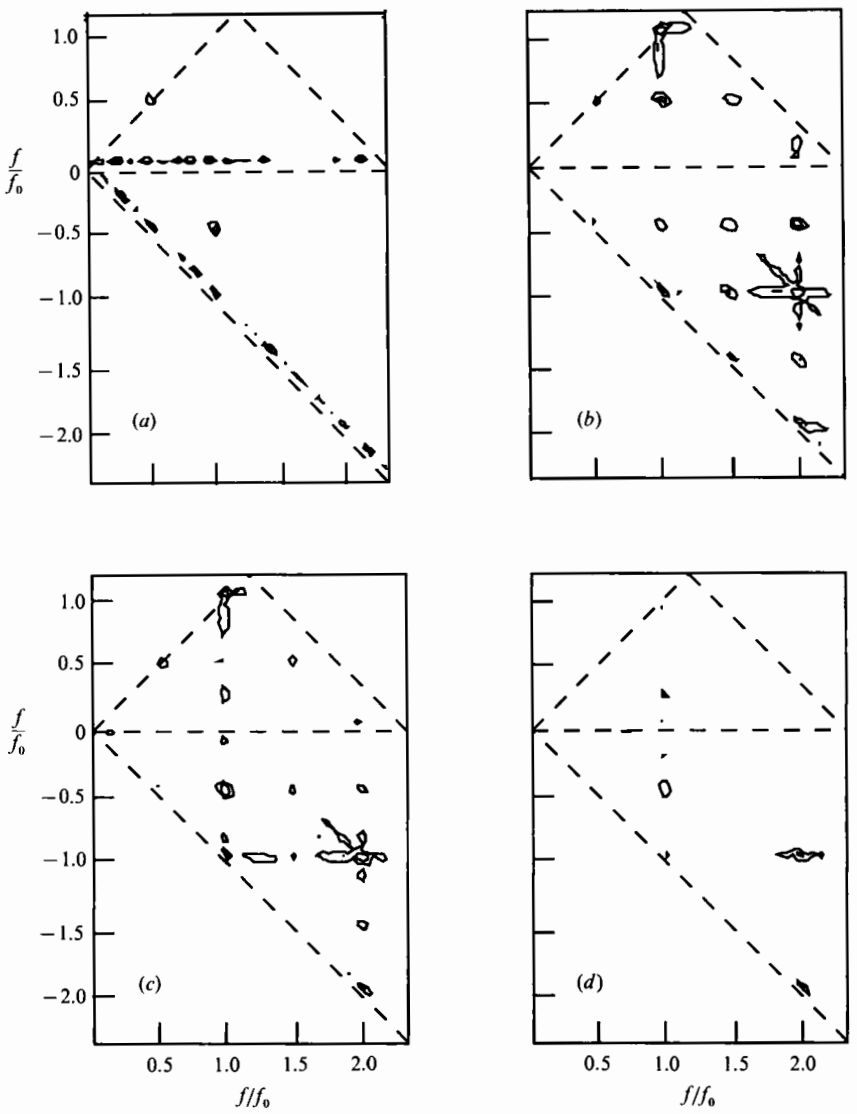

FIGURE 8. Cross-bicoherence spectra, $b^2(f_i, f_j)$, of the longitudinal fluctuations at different downstream locations that correspond to the different regions shown in figure 4. Contour levels are set at 0.3, 0.6, and 0.9. (*a*) Region I, $Rx/\lambda_0 = 0.32$; (*b*) Region II, $Rx/\lambda_0 = 1.6$; (*c*) Region III, $Rx/\lambda_0 = 1.9$; (*d*) Region IV, $Rx/\lambda_0 = 2.3$.

the coupling is a result of the feedback of energy at the fundamental and subharmonic frequencies from the vortex pairing (Corke 1987). In Region II, the level of bicoherence becomes lower as the fundamental starts to equilibrate and the growth rate of the subharmonic mode deviates from its initial exponential growth rate. As the subharmonic starts its second stage of growth in Region III, the level of bicoherence increases again. The existence of phase coupling between the fundamental mode, f_0, and its subharmonic, $\frac{1}{2}f_0$, provides a first step in establishing evidence of a nonlinear coupling or parametric resonance between the fundamental and its subharmonic.

5.2. *Linear and quadratic energy transfer analysis*

The cross-bicoherence analysis provides experimental evidence of the coupling between the fluctuations at the fundamental and subharmonic modes. However, cross-bicoherence measurements alone cannot provide information on the nature and efficiency of the coupling and its role in transferring energy to the subharmonic. It also cannot determine whether the measured three-wave couplings are due to interactions occurring at the location of measurement or are due to earlier upstream interactions which are advected past the probe by the flow. These questions can, to some extent, be answered by measuring the linear and quadratic transfer functions as shown in (5), see also figure 2. If we denote the output of the linear and quadratic transfer functions at frequency f_m by Y_L and Y_Q, respectively, the model output at frequency f_m is then given by

$$\left.\begin{aligned} &Y(f_m) = Y_L(f_m) + Y_Q(f_m), \\ \text{where} \quad &Y_L(f_m) = L(f_m)X(f_m), \quad Y_Q(f_m) = \sum_{f_i \pm f_j = f_m}\sum Q^{f_m}_{f_i,f_j} X(f_i)X(f_j). \end{aligned}\right\} \tag{9}$$

Ritz & Powers (1986) used an iterative approach in the discrete frequency domain to estimate the linear and quadratic transfer functions. A more general approach by Kim & Powers (1988) that does not require iteration was used in our estimates of the linear and quadratic transfer functions. In this approach, the transfer functions are determined by solving two moment equations:

$$E[Y(f_m)X^*(f_m)] = L(f_m)E[X(f_m)X^*(f_m)] + \sum_{f_i \pm f_j = f_m}\sum Q^{f_m}_{f_i,f_j} E[X(f_i)X(f_j)X^*(f_m)] \tag{10}$$

and

$$E[Y(f_m)X^*(f_k)X^*(f_l)] = L(f_m)E[X(f_m)X^*(f_k)X^*(f_l)] + \sum_{f_i \pm f_j = f_m}\sum Q^{f_m}_{f_i,f_j} E[X(f_i)X(f_j)X^*(f_k)X^*(f_l)], \tag{11}$$

where $f_m = f_i \pm f_j = f_k \pm f_l$. Note that these two equations permit one to express the linear transfer function, $L(f_m)$, and the quadratic transfer function, $Q^{f_m}_{f_i,f_j}$ in terms of the various polyspectral moments that can be calculated from the Fourier Transforms of the input and output signals, respectively given by the upstream and downstream sensors of the probe. For example, the two terms on the left-hand sides of (10) and (11) are the cross-power spectrum $S_{xy}(f_m) = E[Y(f_m)X^*(f_m)]$ and the cross-bispectrum $S_{yxx}(f_k, f_l) = E[Y(f_m)X^*(f_k)X^*(f_l)]$. The terms on the right-hand sides are a hierarchy of spectral moments, specifically, the auto-power spectrum $S_{xx}(f_m) = E[X(f_m)X^*(f_m)]$, the auto-bispectrum $S_{xxx}(f_k, f_l) = E[X(f_m)X^*(f_k)X^*(f_l)]$ and a fourth-order spectral moment of the input $E[X(f_i)X(f_j)X^*(f_k)X^*(f_l)]$.

Once the linear and quadratic transfer functions are determined, one can predict the output spectrum, $\hat{S}_{yy}(f_m)$, as

$$\begin{aligned} \hat{S}_{yy}(f_m) &= E[Y(f_m)\,Y^*(f_m)] = E[(Y_L(f_m) + Y_Q(f_m))\,(Y_L(f_m) + Y_Q(f_m))^*] \\ &= E[Y_L(f_m)\,Y_L^*(f_m)] + E[Y_Q(f_m)\,Y_Q^*(f_m)] + 2\,\mathrm{Re}\,E[Y_L(f_m)\,Y_Q^*(f_m)] \\ &= S_L(f_m) + S_Q(f_m) + S_{LQ}(f_m), \end{aligned} \tag{12}$$

where $$S_L(f_m) = |L(f_m)|^2 E[|X(f_m)|^2] = |L(f_m)|^2 S_{xx}(f_m),$$

$$S_Q(f_m) = \sum_{f_i \pm f_j = f_m} \sum_{f_k \pm f_l = f_m} \{Q^{f_m}_{f_i;f_j} Q^{f_m *}_{f_k;f_l} E[X(f_i) X(f_j) X^*(f_k) X^*(f_l)]\},$$

and $$S_{LQ}(f_m) = 2\,\mathrm{Re}\Big[\sum_{f_i \pm f_j = f_m} L(f_m)\, Q^{f_m *}_{f_i;f_j} E[X(f_m) X^*(f_i) X^*(f_j)]\Big].$$

The 'predicted' output power spectrum is then the sum of the linear power spectrum, $S_L(f_m)$, the 'quadratic' power spectrum, $S_Q(f_m)$, and a linear–quadratic power spectrum, $S_{LQ}(f_m)$. It is important to note here that, in the set-up of the probe used in these experiments, the output power $S_{yy}(f_m)$ includes the input power $S_{xx}(f_m)$ which is advected by the mean flow from the first sensor to the second sensor. Because our interest is in the local characteristics of the linear and nonlinear growth mechanisms, we subtract the input power from the output power and consider only the change in the power spectrum, $\Delta S(f)$, between the two streamwise locations:

$$\begin{aligned}\Delta S(f_m) &= \hat{S}_{yy}(f_m) - S_{xx}(f_m) = S_L(f_m) - S_{xx}(f_m) + S_Q(f_m) + S_{LQ}(f_m) \\ &= [|L(f_m)|^2 - 1] S_{xx}(f_m) + S_Q(f_m) + S_{LQ}(f_m) \\ &= S'_L(f_m) + S_Q(f_m) + S_{LQ}(f_m), \end{aligned} \tag{13}$$

where $S'_L(f_m) = [|L(f_m)|^2 - 1] S_{xx}(f_m)$. In this equation, the change in the energy content of the mode with frequency f_m is divided into three parts, namely the linear, quadratic, and linear–quadratic changes.

A power transfer rate, $\tau^2(f_m)$, can then be defined as the ratio of the estimated change in the energy of the mode with frequency f_m and the actual input energy of that mode over the distance Δx, $\Delta S(f_m)/(S_{xx}(f_m)\,\Delta x)$. The power transfer rate can then be divided into three parts, namely the linear power transfer rate, $\tau^2_l(f_m) = [|L(f_m)|^2 - 1]$, the quadratic power transfer rate, $\tau^2_q(f_m)$, and the linear–quadratic power transfer rate, $\tau^2_{lq}(f_m)$. These are given as the ratios of $S'_L(f_m)$, $S_Q(f_m)$ and $S_{LQ}(f_m)$ over $S_{xx}(f_m)$, respectively. For a perfect system with no errors, all the energy change is accounted for by the three parts and the power transfer rate is equal to one. Also, as noted in §4, the linear transfer component, $\tau^2_l(f_m)$, includes the effect of the linear growth and the energy transfer via the parametric mechanism to the mode of frequency f_m. The transfer of energy via nonlinear resonance of two input modes f_i and f_j to an output mode at f_m is included in the quadratic power transfer component, $\tau^2_q(f_m)$.

5.2.1. *Quadratic energy transfer*

As noted in §4, the nonlinear transfer of energy from two input modes f_i and f_j to an output mode at f_m depends on the quadratic transfer function $Q^{f_m}_{f_i;f_j}$. This quantity is a complex function with amplitude and phase. From (5), it can be shown that the quadratic transfer function is given by

$$Q^{f_m}_{f_i;f_j} = (Y(f_m) - L(f_m) X(f_m))/X(f_i) X(f_j), \quad f_m = f_i \pm f_j. \tag{14}$$

Note that the quadratic transfer function is inversely dependent on the amplitudes of input modes, $X(f_i)$ and $X(f_j)$. Figure 9 shows the logarithmic contour plots of the magnitude of the quadratic transfer functions, $|Q^{f_m}_{f_i;f_j}|^2$, measured at locations that correspond to the four regions defined above. Note that the overall details of $|Q^{f_m}_{f_i;f_j}|^2$ plots change gradually in the downstream direction. For instance, the magnitude of the quadratic transfer function is very low at $(f_0, -\frac{1}{2}f_0)$, at each downstream location. From (14), it is evident that this is in part due to the fact that the energy

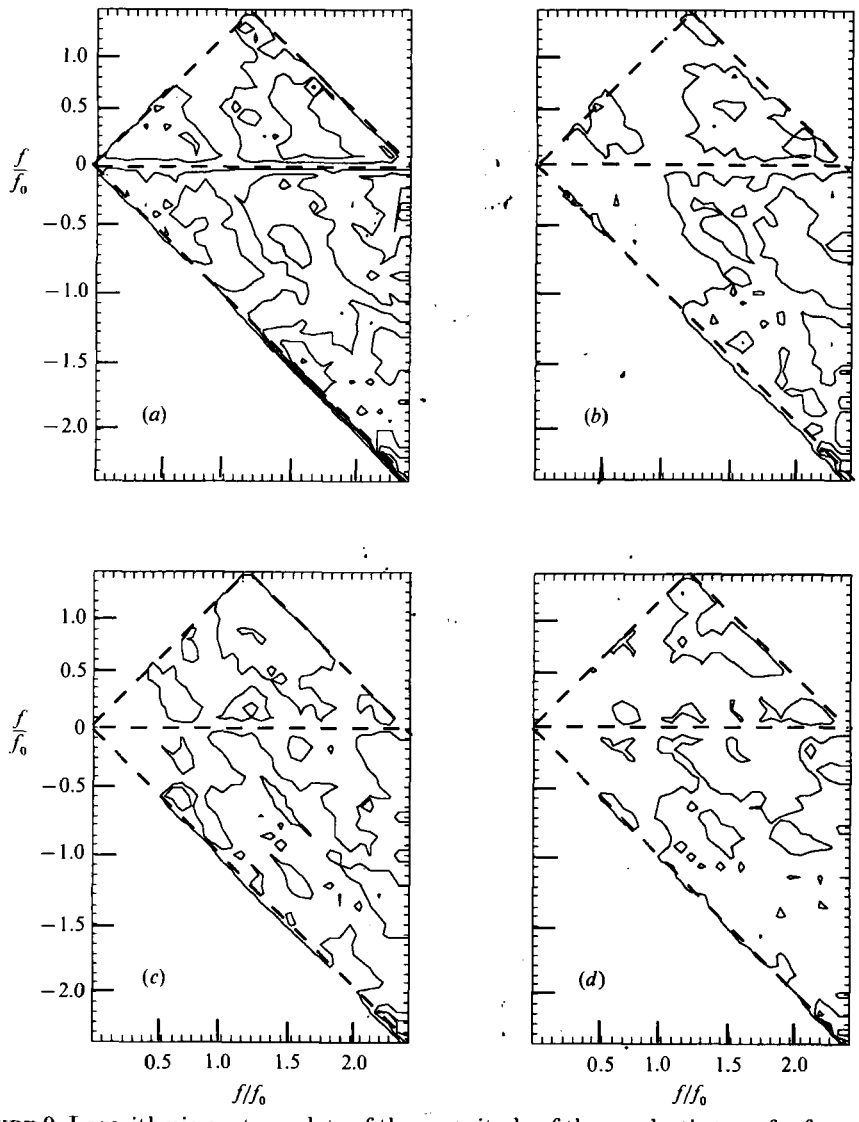

FIGURE 9. Logarithmic contour plots of the magnitude of the quadratic transfer functions, $|Q^m_{f_i,f_j}|^2$, of the longitudinal fluctuations at different downstream locations that correspond to the different regions shown in figure 4. Contour levels are set at 0.5, 1.5, and 2.5. (*a*) Region I, $Rx/\lambda_0 = 0.32$; (*b*) Region II, $Rx/\lambda_0 = 1.6$; (*c*) Region III, $Rx/\lambda_0 = 2.6$; (*d*) Region IV, $Rx/\lambda_0 = 3.2$.

of the input modes at f_0 and $\frac{1}{2}f_0$ is large. However, it is important to note that, although the large energy levels at f_0, $\frac{1}{2}f_0$ and $\frac{3}{2}f_0$ are comparable, the magnitude of the quadratic transfer function is larger at $(\frac{3}{2}f_0, -f_0)$ and $(2f_0, -f_0)$ than at $(f_0, -\frac{1}{2}f_0)$. This suggests that the efficiency of the quadratic energy transfer via nonlinear resonance is larger for the $(\frac{3}{2}f_0, -f_0)$ and $(2f_0, -f_0)$ interactions than for the $(f_0, -\frac{1}{2}f_0)$ (i.e. fundamental—subharmonic) interaction. The sensitivity of the quadratic transfer function to the energy level of the input modes is also apparent from the fact that, at all downstream locations, measured values of the quadratic transfer function magnitude are typically large for pairs of frequency components that have low input energy. This effect stems from the fact that the quadratic transfer function is

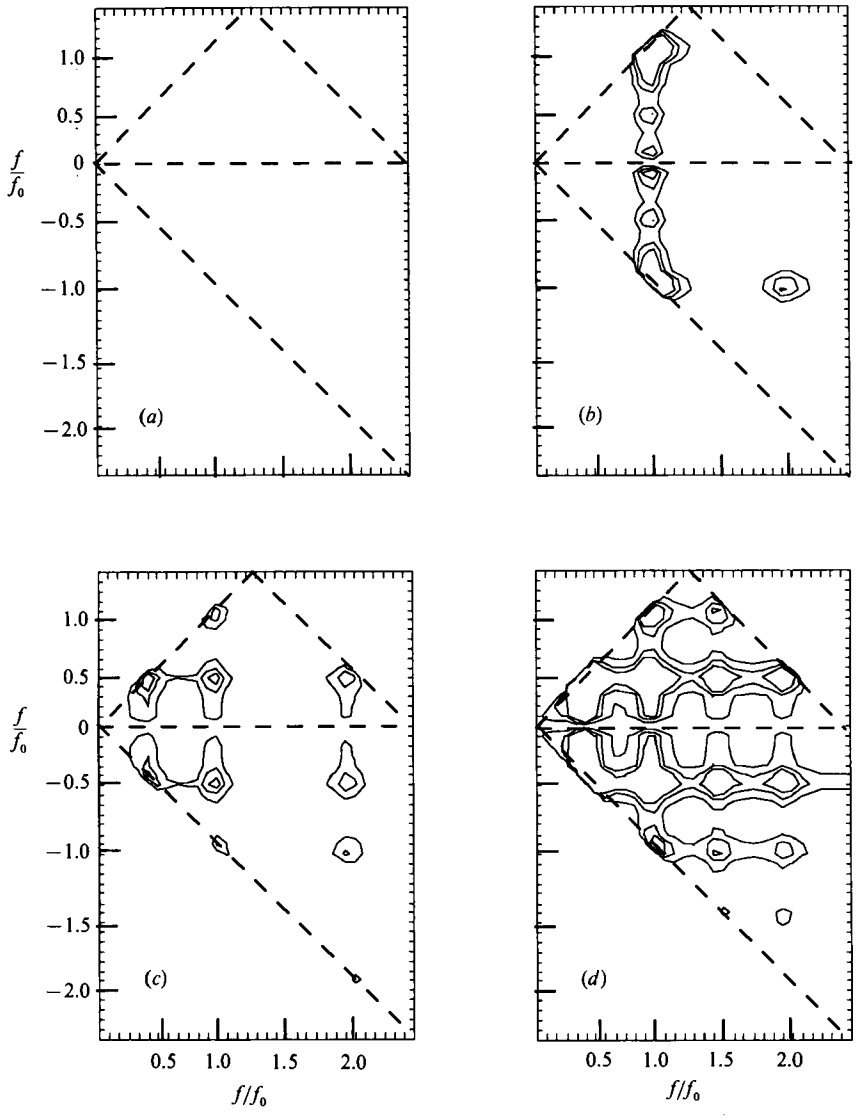

FIGURE 10. Contours plots of the interaction potential, $|X(f_i)X(f_j)|^2$, of the longitudinal fluctuations at different downstream locations that correspond to the different regions shown in figure 4. Contour levels are set at 0.2, 0.5, and 0.8. (*a*) Region I, $Rx/\lambda_0 = 0.32$; (*b*) Region II, $Rx/\lambda_0 = 1.6$; (*c*) Region III, $Rx/\lambda_0 = 2.6$; (*d*) Region IV, $Rx/\lambda_0 = 3.2$.

dimensional, as evident by (14), and is inversely dependent on the energy level of the interacting modes.

Miksad, Hajj & Powers (1989) proposed that a good measure of the amplitude dependence of $Q^{f_m}_{f_i,f_j}$ is given by the magnitude of the coupled input energy level, $|X(f_i)X(f_j)|^2$, which will be referred to as the 'interaction potential'. This quantity is a measure of the potential amount of energy that interacting modes have for nonlinear energy transfer. Low-energy modes have less energy to transfer to a third mode than high-energy modes do. Figure 10 shows the frequency domain distribution of the interaction potential at four downstream locations that correspond to the different regions of the transition, as defined in §3. Note that the upper and lower

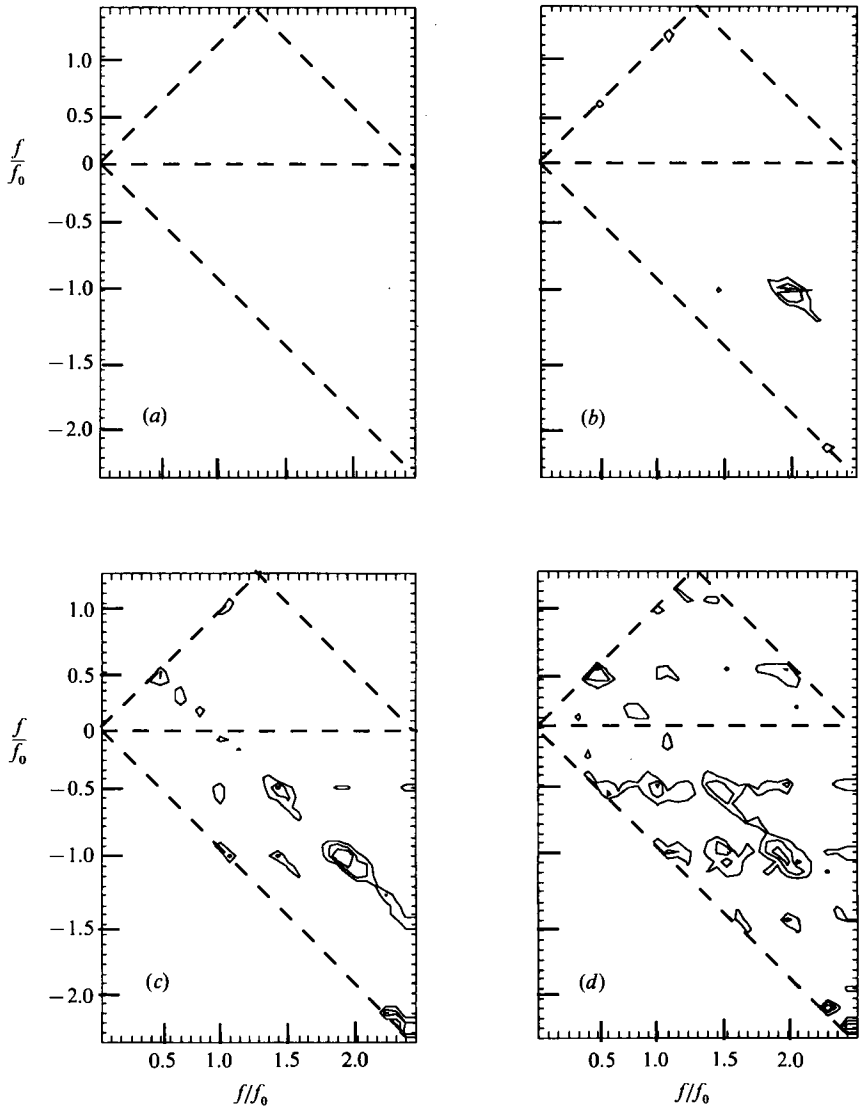

FIGURE 11. Contours of the weighted non-dimensional quadratic transfer functions, $Q'^2(f_i, f_j)$, of the longitudinal fluctuations along $\max u'_{\text{rms}}$ under natural excitation at different downstream locations that correspond to the different regions shown in figure 4. Contour levels are set at 0.3, 0.6, and 0.9. (*a*) Region I, $Rx/\lambda_0 = 0.32$; (*b*) Region II, $Rx/\lambda_0 = 1.6$; (*c*) Region III, $Rx/\lambda_0 = 2.6$; (*d*) Region IV, $Rx/\lambda_0 = 3.2$.

triangular regions are symmetrical, since $X(-f) = X^*(f)$ and therefore $|X(-f)|^2 = |X(f)|^2$. Note that in Region II, most of the interaction potential is centred at (f_0, f_0) indicating a significant input potential for the transfer of energy to the first harmonic. The actual energy transfer the first harmonic can be clearly seen in the power spectra and bicoherence plots. The large interaction potential at $(f_0, -\frac{1}{2}f_0)$ indicates that significant energy transfer to the subharmonic can also occur in these regions.

A measure of nonlinear energy transfer can be obtained by weighting the dimensional quadratic transfer function, $Q^{f_m}_{f_i,f_j}$, by the energy potential of the

interacting input modes, $|X(f_i)X(f_j)|^2$, to obtain a non-dimensional quadratic transfer function such as

$$Q'^2(f_i,f_j) = E[|Q^{f_m}_{f_i,f_j}|^2 (|X(f_i)X(f_j)|^2)^{\frac{1}{2}}], \quad f_m = f_i \pm f_j. \tag{15}$$

Contour plots of the weighted non-dimensional transfer functions, along maximum $u'_{\rm rms}$, are shown in figure 11. Pairs that show high $Q'^2(f_i,f_j)$ characterize those interactions which are potentially most efficient in transferring energy. Note that, at $Rx/\lambda_0 = 0.32$, there are no indications of any prospect for energy transfer between any components. This location corresponds to Region I, the region of primary instability. These results agree with the predictions of the linear stability theory that all modes grow independently in the early region of the transition. More important to the question of subharmonic generation is the fact that although the cross-bicoherency plots indicate nonlinear coupling starting at $Rx/\lambda_0 = 0.32$, the $|Q'|^2$ measurements indicate that the prospect for quadratic energy transfer to the subharmonic in this region is not significant. This demonstrates that the growth of the subharmonic in Region I is not due to a nonlinear interaction mechanism. The first involvement of the subharmonic in nonlinear interaction appears in the sum region at $Rx/\lambda_0 = 1.6$, at the end of Region II. Recall that by this location, the fundamental has started to equilibrate and the subharmonic growth rate has deviated from its initial exponential growth. However, the involvement of the subharmonic component in nonlinear energy transfer does not become significant until $Rx/\lambda_0 = 2.6$, where the contour levels of $|Q'|^2$ at $(f_0, -\frac{1}{2}f_0)$ and $(\frac{3}{2}f_0, -f_0)$ are larger than at earlier locations. This indicates that, up to this location, the prospect for quadratic energy transfer to the subharmonic is very low. Further downstream, at $Rx/\lambda_0 = 3.2$ in Region III, the subharmonic, the fundamental and their harmonics have entered into a wide variety of interactions with other fluctuations and the $|Q'|^2$ contours indicate the initiation of a redistribution of subharmonic and fundamental mode energy to the different components of the flow.

5.2.2. *Linear and parametric energy transfer*

The above measurements of the quadratic transfer function and its weighted non-dimensional function show an important result. Both the quadratic transfer function, $|Q|^2$, and its weighted form, $|Q'|^2$ show large magnitudes at $(2f_0, -f_0)$. This indicates efficient transfer of energy between these modes. On the other hand, the level of the magnitudes of these functions at the fundamental–subharmonic, $(f_0, -\frac{1}{2}f_0)$, indicate that the prospects for quadratic transfer of energy due to nonlinear resonance from the fundamental to the subharmonic are low. The question that arises is then: What is the role of the linear transfer function that includes the parametric effects on the growth of the subharmonic? This question can be answered by examining the linear transfer function and its role in the transfer of energy to the subharmonic and by comparing it to the corresponding role of the quadratic transfer function.

The growth rate of the fundamental, subharmonic and $\frac{3}{2}$ harmonic due to linear and linear-like effects, at different downstream locations, are given by the plot of the linear power transfer rate, $\tau_l^2(f_m)$, as shown in figure 12. Note that, in Region I, the linear power transfer rates of the three modes are constant and equal to the growth rates as predicted by the linear instability theory of Monkewitz & Huerre (1982). In Region II, between $Rx/\lambda_0 = 1.0$ and $Rx/\lambda_0 = 1.6$, the level of the linear power transfer rate, $\tau_l^2(f_m)$, of these modes starts to decrease. This decrease in the growth of these modes is expected because of the spreading of the mixing layer. Beyond

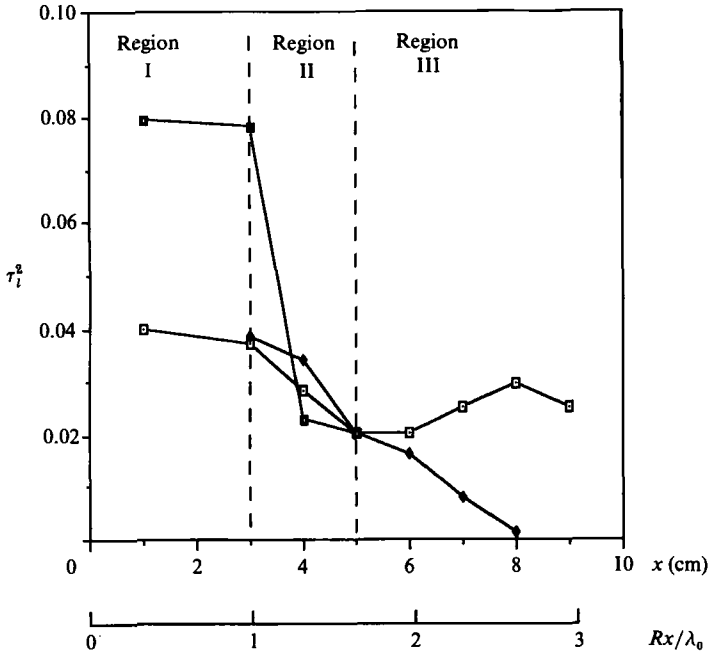

FIGURE 12. Linear power transfer rate, $\tau_l^2(f)$, of the fundamental, f_0 (—■—), the subharmonic, $\frac{1}{2}f_0$(—⊡—) and the $\frac{3}{2}$ harmonic, $\frac{3}{2}f$ (—◆—) *vs.* downstream distance.

Region II, only the linear power transfer of the subharmonic and $\frac{3}{2}$ harmonic are shown. The fundamental growth is negative and therefore is not shown. In Region III, between $Rx/\lambda_0 = 1.6$ and $Rx/\lambda_0 = 2.6$, the linear power transfer rate, $\tau_l^2(f_m)$, of the $\frac{3}{2}$ harmonic continues to decrease. In contrast, the linear power transfer rate of the subharmonic increases. Only a linear-like mechanism, such as the parametric mechanism, may explain the increase in the linear power transfer rate of the subharmonic. These results indicate that the growth of the subharmonic in Region III is accompanied by an increase in the linear transfer of power as a result of the parametric resonance mechanism.

The total energy change of the subharmonic, $\Delta S(\frac{1}{2}f_0)$ at different downstream locations is shown in figure 13(*a*). Also shown on the same plot are the portions of $\Delta S(\frac{1}{2}f_0)$ that are due to linear and quadratic effects, $S_L(\frac{1}{2}f_0)$ and $S_Q(\frac{1}{2}f_0)$, respectively. Since the parametric resonance mechanism is a linear-like mechanism, its activity will appear in the linear term of (5). The transfer of energy to the subharmonic due to nonlinear interactions, $S_Q(\frac{1}{2}f_0)$, is two to three orders of magnitude less than the energy transfer by parametric linear-like mechanisms, $S_L(\frac{1}{2}f_0)$. Although both parametric and nonlinear mechanisms are simultaneously influencing the subharmonic, the results clearly show that the change in the power of the subharmonic mode is mainly due to a parametric resonance and only small nonlinear effects are present.

The nature of the energy transfer to the $\frac{3}{2}$ harmonic in Region III stands in contrast to that of the subharmonic. Figure 13(*b*) shows the total output energy change of the $\frac{3}{2}$ harmonic, $\Delta S(\frac{3}{2}f_0)$ at different downstream locations. The contributions of $S_L(\frac{3}{2}f_0)$ and $S_Q(\frac{3}{2}f_0)$ to the overall energy change, $\Delta S(\frac{3}{2}f_0)$, are also shown on the same figure. Note that in Region I the linear energy transfer to $\frac{3}{2}f_0$, $S_L(\frac{3}{2}f_0)$, is dominant. However, as we move further downstream to Region III,

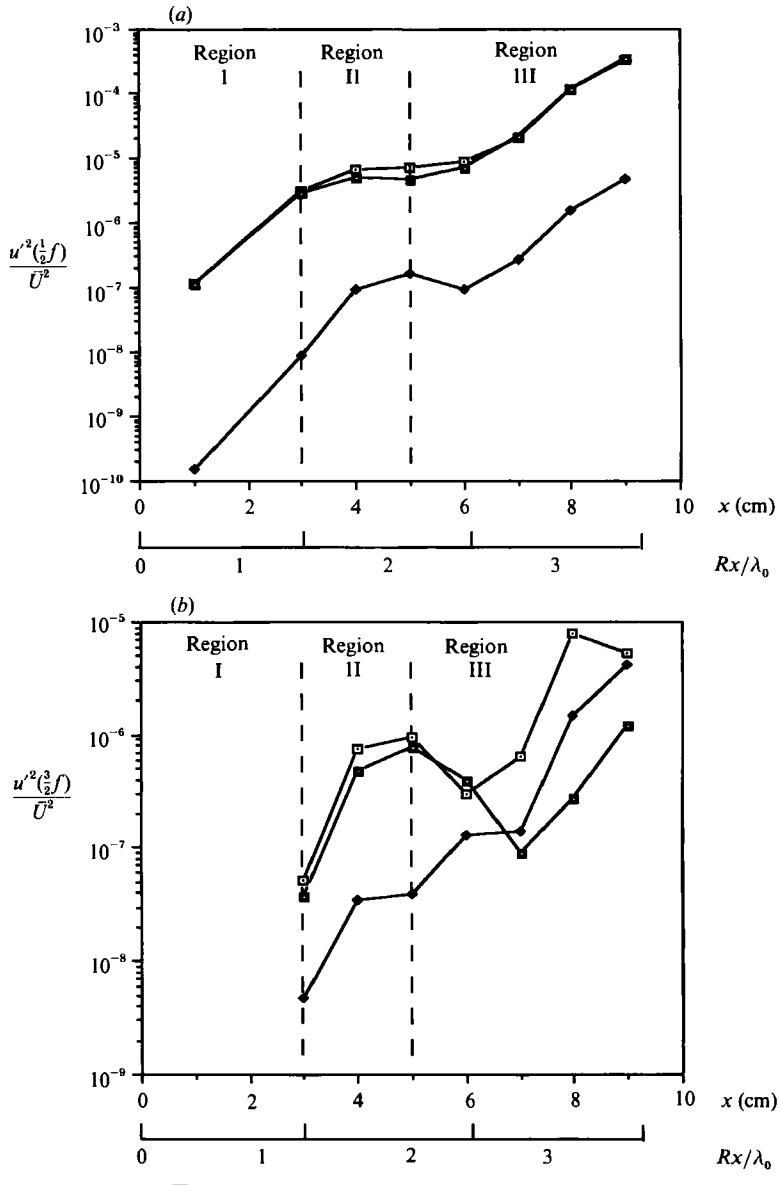

FIGURE 13(a, b). For caption see facing page.

quadratic energy transfer to $\frac{3}{2}f_0, S_Q(\frac{3}{2}f_0)$, becomes the dominant factor. This suggests that nonlinear interactions are more important in Region III in transferring energy to $\frac{3}{2}f_0$ than are parametric or linear mechanisms.

The differences between the mechanisms responsible for the energy transfer to the subharmonic and to the $\frac{3}{2}$ harmonic are also evident in the comparisons of the ratio of the quadratic to linear contributions, S_Q/S_L, for $\frac{1}{2}f_0$ and $\frac{3}{2}f_0$ at the different downstream locations, as shown in figure 13(c). Notice that while this ratio is of the order of 0.001 to 0.01 in the case of the subharmonic, $\frac{1}{2}f_0$, it is of the order of 0.1 to 10 in the case of $\frac{3}{2}f_0$, depending on the downstream location. This again suggests that,

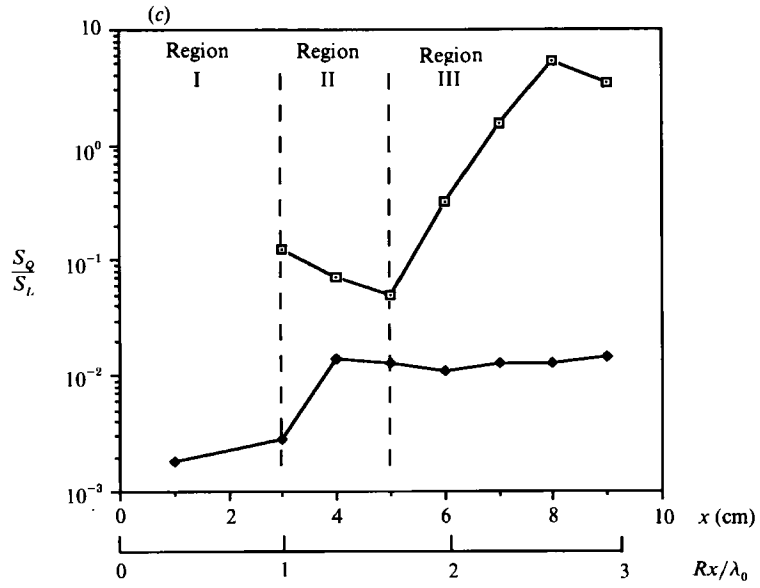

FIGURE 13. (*a*) Total power change, $\Delta S(\frac{1}{2}f_0)$, and linear and quadratic power transfer, $S_L(\frac{1}{2}f_0)$ and $S_Q(\frac{1}{2}f_0)$, respectively, *vs.* downstream distance; and Total power change, $\Delta S(\frac{3}{2}f_0)$, and linear and quadratic power transfer, $S_L(\frac{3}{2}f_0)$ and $S_Q(\frac{3}{2}f_0)$, respectively, *vs.* downstream distance (—⊡—, ΔS; —■—, S_L; —◆—, S_Q). (*c*) Ratio of quadratic to linear power transfer rate of the subharmonic, $\frac{1}{2}f_0$ (—◆—), and the $\frac{3}{2}$ harmonic, $\frac{3}{2}f_0$ (—⊡—) *vs.* downstream distance.

in Region III, nonlinear interactions are primarily responsible for the growth of $\frac{3}{2}f_0$ and that parametric effects are primarily responsible for subharmonic growth.

5.3. *Wavenumber–frequency matching*

The spatial characteristics of the transitioning mixing layer are obtained using the technique described in §4. These characteristics are seen in the estimates of the local wavenumber–frequency spectra $S(k, f)$ that are shown in figure 14. From these plots we can detect some features of the dispersion relationship. At $Rx/\lambda_0 = 0.32$, only the fundamental and subharmonic modes have a definite dispersion relationship. By $Rx/\lambda_0 = 1.6$, we notice the generation of the second harmonic. Also notice that the harmonic bands, at f_0, $\frac{1}{2}f_0$ and $2f_0$ are confined to a relatively narrow range of wavenumbers. By $Rx/\lambda_0 = 2.3$, we notice the broadening of the spectrum along the harmonic components and the valleys.

In order to gain better insight into the spatial characteristics of the different components of the flow, plots of the local wavenumber spectra are shown in figure 15. In the primary instability region or Region I, at $Rx/\lambda_0 = 1.0$, most of the energy is contained in a band of wavenumbers centred at $k_0 = 3.4$ rad/cm, which corresponds to a wavelength of 1.83 cm. This value is very close to the wavelength of the fundamental instability, $\lambda_0 = 1.98$ cm. By $Rx/\lambda_0 = 2.3$, or in Region II, different wavenumber components have gained some energy, leading to broadening of the spectrum. In Region III, between $Rx/\lambda_0 = 2.6$ and 3.2, the wavenumber spectra show that most of the energy is contained in a band of wavenumbers centred at $k = 1.7$ rad/cm ($= \frac{1}{2}k_0$), which is half the value at which the initial peak is located. Therefore, as the maximum energy in the frequency spectrum, in figure 6, shifts from f_0 to $\frac{1}{2}f_0$, the peak in the wavenumber spectra, in figure 15, shifts from k_0 to $\frac{1}{2}k_0$. This

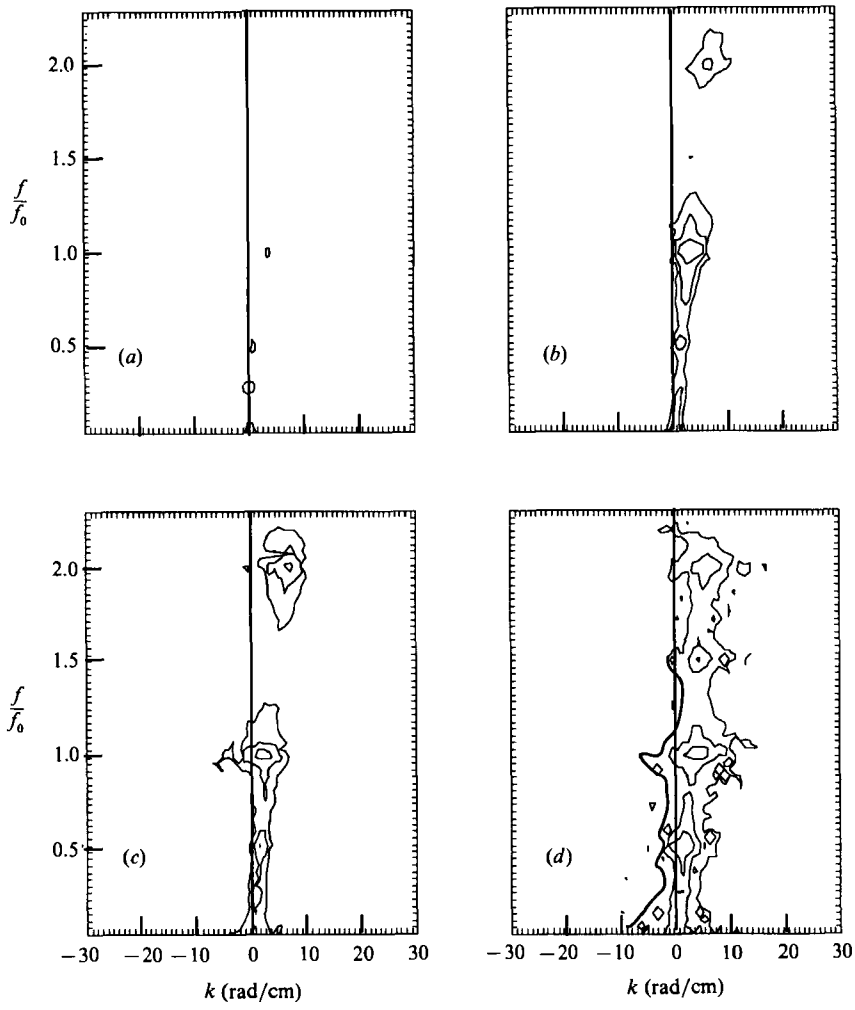

FIGURE 14. Wavenumber–frequency spectra, $S(k, f)$, of the longitudinal fluctuations at different downstream locations that correspond to the different regions shown in figure 4. Contour levels are set at 10^{-6}, 10^{-5}, and 10^{-4}. (*a*) $Rx/\lambda_0 = 0.32$; (*b*) 1.6; (*c*) 2.3; (*d*) 3.2.

shift occurs after the primary instability region of the transition, and coincides with the second region of subharmonic growth. The merging of the two vortices reduces the frequency of their passage from f_0 to $\frac{1}{2}f_0$ and increases their characteristic size from $l_0 = 2\pi/k_0$ to $2l_0$. The shifting of the centre of the band from k_0 to $\frac{1}{2}k_0$ represents an increase in the characteristic size of the vortices and therefore provides a spatial indication of the vortex merging process.

An important condition for parametric resonance to take place is that the subharmonic and the fundamental modes travel at the same phase speed. This condition was assumed by Kelly (1967) and postulated by Monkewitz (1988). Figure 16 shows the variation of the normalized phase speeds, $(\omega/k)/\bar{U}$, of the fundamental and the subharmonic in the downstream direction. Notice the good matching between the two modes beyond $Rx/\lambda_0 = 1.6$ (i.e. Region III). This shows that the condition of wavenumber resonance is satisfied beyond the initial region of growth

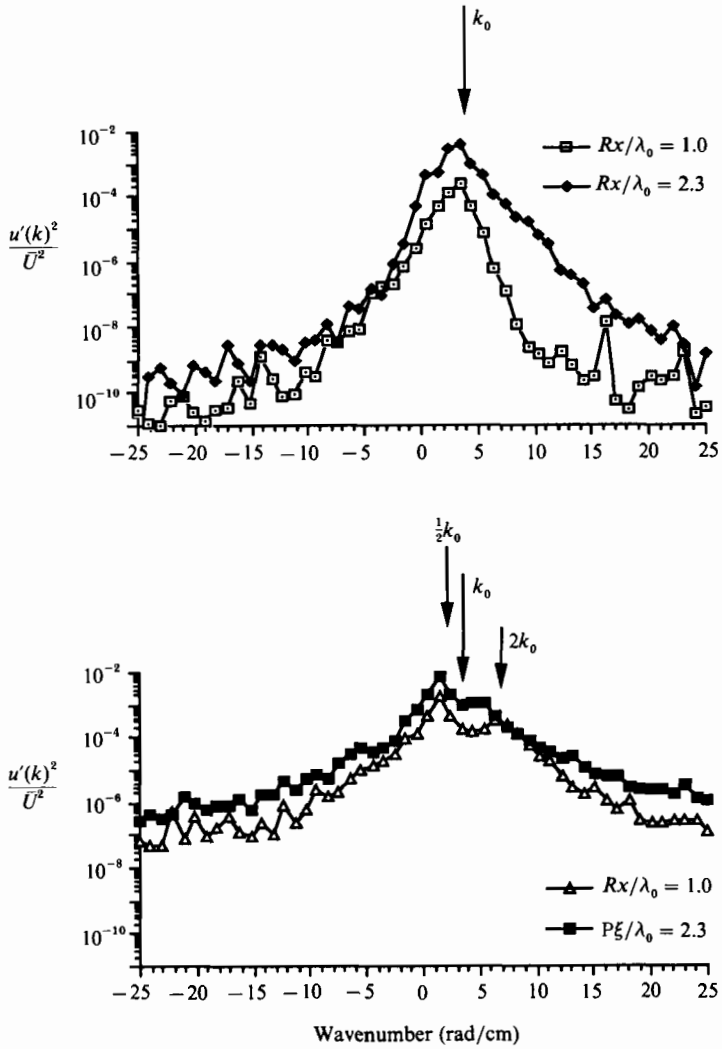

FIGURE 15. Wavenumber spectra of the longitudinal fluctuations at downstream locations that correspond to the different regions shown in figure 4.

of the subharmonic. This is in agreement with the requirements of the analysis of Kelly (1967) and Monkewitz (1988).

Monkewitz (1988) showed that the amplitude of the fundamental mode must attain a critical value before it becomes phase locked with the subharmonic and the growth rate of the subharmonic is modified. At this location the phase speed of the subharmonic is close to unity, i.e. the phase speed of the neutral fundamental. Monkewitz (1988) also showed that when the fundamental amplitude is larger than or equal to the critical amplitude, the growth of the subharmonic and its phase speed are dependent on the phase difference, $\Delta\phi$, between the fundamental and the subharmonic (see figures 6 and 7 in Monkewitz 1988). These figures show that the optimal conditions for the subharmonic growth occur when the phase difference between the two modes is close to zero. Monkewitz also showed that when the fundamental amplitude is decreasing, the growth of the subharmonic is enhanced regardless of the initial phase difference (see figure 9 in Monkewitz 1988). The results

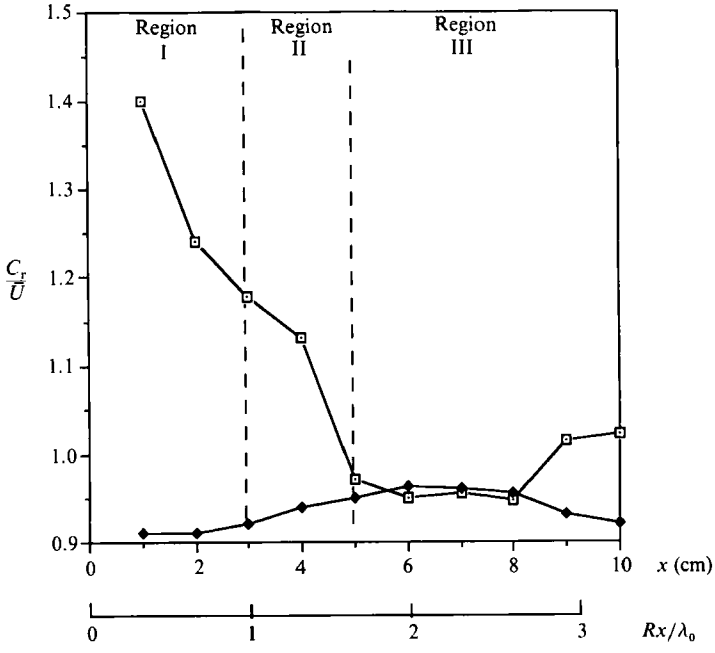

FIGURE 16. Downstream variations of the normalized phase speed, $C_r/\bar{U}$, of the fundamental (—◆—) and subharmonic (—⊡—) modes.

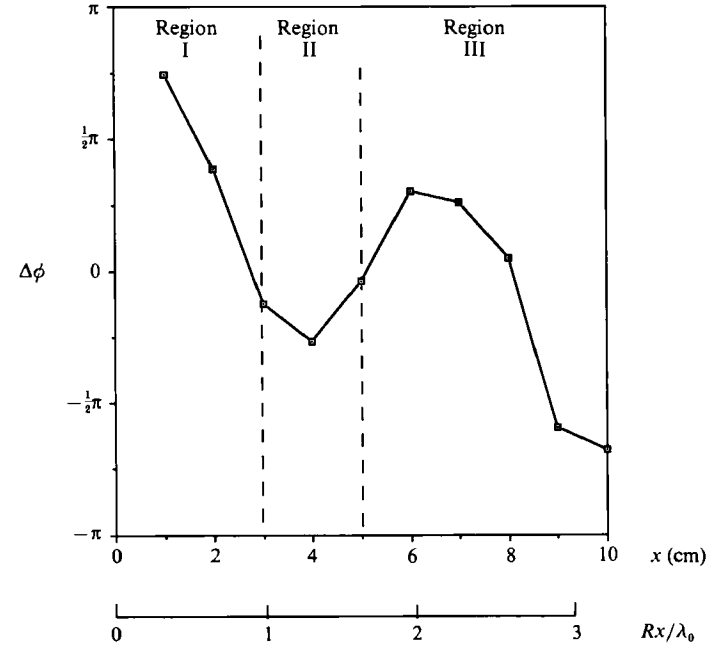

FIGURE 17. Downstream variations of the phase difference, $\Delta\phi$, between the fundamental and subharmonic modes.

of our experiments show that when the fundamental reaches its critical amplitude the growth rate of the subharmonic is decreasing, the phase speed of the subharmonic is not equal to unity and the energy transfer between the fundamental and the subharmonic is not efficient. However, these conditions for the subharmonic growth are met further downstream, beyond $Rx/\lambda_0 = 1.6$. Figure 17 shows the variation in the phase difference between the fundamental and the subharmonic in the downstream direction. At $Rx/\lambda_0 = 1.0$, where the fundamental amplitude is close to the critical amplitude, the phase difference between the fundamental and the subharmonic close to zero. By comparison to figure 6 of Monkewitz (1988), we note that at this phase difference, the growth of the subharmonic is suppressed over a small distance before it starts growing again. The reduced growth rate at $Rx/\lambda_0 = 1.0$ agrees with the predictions of Monkewitz (1988). At $Rx/\lambda_0 = 1.6$, where the fundamental amplitude is equal to five times the critical amplitude, the phase difference is still close to zero. By comparison with figure 7 of Monkewitz (1988), we note that the subharmonic growth is reduced at this phase angle. This also agrees with the reduced growth rate at this location as seen in figure 4. This reduced growth is also due to the low bicoherence (figure 7) which indicates low coupling and large phase difference variations. Further downstream, at $Rx/\lambda_0 = 2.3$, the amplitude of the fundamental is equal to twice that of the critical amplitude. The subharmonic amplitude is increasing significantly. However the fundamental amplitude is decreasing. By comparison with figure 9 of Monkewitz (1988), we note that the subharmonic should be growing at any phase difference. This result also agrees with the energy transfer measurements that show efficient energy transfer from the fundamental to the subharmonic at this location.

6. Conclusions

The nonlinear and parametric characteristics that are associated with the subharmonic generation in the transition to turbulence in plane mixing layers are detected and quantified. In the primary instability region of the transition, all instability modes, including the subharmonic, grow independently. No significant transfer of energy between any modes is detected. Measurements of the power spectra and the associated linear and quadratic transfer functions show that beyond this initial region, the spatial growth of the subharmonic supports the parametric approach which is described by a linear model with varying time coefficients. On the other hand, the same measurements show that the growth of $2f_0$ and $\frac{3}{2}f_0$ is best described by the quadratic nonlinear interaction approach. The growth rate of the subharmonic starts modifying about the location where $Rx/\lambda_0 \approx 1$. At this location, the fundamental amplitude is equal to $0.012\bar{U}$ and has not yet started to saturate. This shows that the parametric resonance between the fundamental and the subharmonic can start to affect subharmonic growth before the fundamental reaches its saturation amplitude. However, the most efficient transfer of energy to the subharmonic occurs further downstream as the fundamental mode reaches an amplitude close to its saturation amplitude. Measurements also indicate that the fundamental, besides interacting with the subharmonic, is also engaged in redistributing its energy via nonlinear interactions to other components such as the first harmonic and the valleys. Local wavenumber measurements verify that frequency–wavenumber resonance matching conditions exist between the fundamental and subharmonic in regions where efficient energy exchange to the subharmonic takes place. These results are in general agreement with theoretical models by Kelly (1967) and Monkewitz (1988).

This paper is based in part upon work supported by the Texas Advanced Technology Program under Grant No. ATP 3280, and in part by the National Science Foundation under Grant No. MSM-8211205. The digital signal processing techniques were developed under the auspices of the Department of Defense Joint Services Electronics Program under the Air Force Office of Scientific Research (AFOSR) Contract No. F49620-89-C-0044.

REFERENCES

BEALL, J. M., KIM, Y. C. & POWERS, E. J. 1982 Estimation of wavenumber and frequency spectra using fixed probe pairs. *J. Appl. Phys.* **53**, 3933–3940.

BRETHERTON, F. P. 1964 Resonant interactions between waves. The case of discrete oscillations. *J. Fluid Mech.* **20**, 457–479.

BROWAND, F. K. 1966 An experimental investigation of the instability of an incompressible separated shear layer. *J. Fluid Mech.* **26**, 281–307.

BROWN, G. L. & ROSHKO, A. 1974 On density effects and large structure in turbulent mixing layers. *J. Fluid Mech.* **64**, 775–816.

CORKE, T. C. 1987 Measurements of resonant phase locking in unstable axisymmetric jets and boundary layers. In *Nonlinear Wave Interactions in Fluids* (ed. R. W. Miksad, T. R. Akylas & T. Herbert). The Winter Annual Meeting of ASME, AMD vol. 87, pp. 37–65.

HO, C. M. 1982 Local and global dynamics of free shear layers. In *Proc. Symp. on Numerical and Physical Aspects of Aerodynamics Flow* (ed. T. Cebeci), pp. 521–533. Springer.

HO, C. M. & HUANG, L. S. 1982 Subharmonics and vortex merging in mixing layers. *J. Fluid Mech.* **119**, 443–473.

HO, C. M. & HUERRE, P. 1984 Perturbed free shear layers. *Ann. Rev. Fluid Mech.* **16**, 365–424.

HUANG, L. S. & HO, C. M. 1990 Small-scale transition in a plane mixing layer. *J. Fluid Mech.* **210**, 475–500.

ITOH, N. 1977 Nonlinear stability of parallel flows with subcritical Reynolds numbers. Part 1. An asymptotic theory valid for small amplitude disturbances. *J. Fluid Mech.* **82**, 455–467.

JONES, F. L. 1983 An experimental study of nonlinear wave interactions and modulations during transition of a symmetric wake. Ph.D. dissertation, LTT-83-02, The University of Texas at Austin.

JONES, F. L., RITZ, C. P., MIKSAD, R. W., POWERS, E. J. & SOLIS, S. R. 1988 Measurement of the local wavenumber and frequency spectrum in a plane wake. *Exps. in Fluids* **6**, 365–372.

KELLY, R. E. 1967 On the stability of an inviscid shear layer which is periodic in space and time. *J. Fluid Mech.* **27**, 657–689.

KIM, K. I. & POWERS, E. J. 1988 A digital method of modeling quadratically nonlinear systems with a general random input. *IEEE Trans. Acoust., Speech, Signal Process.* **36**, 1758–1769.

MIKSAD, R. W. 1972 Experiments on the non-linear stages of free shear layer transition. *J. Fluid Mech.* **56**, 695–719.

MIKSAD, R. W. 1973 Experiments on nonlinear interactions in the transition of a free shear layer. *J. Fluid Mech.* **59**, 1–21.

MIKSAD, R. W., HAJJ, M. R. & POWERS, E. J. 1989 Measurements of nonlinear transfer functions for subharmonic generation in mixing layers. *AIAA* 89-0980.

MIKSAD, R. W., JONES, F. L., POWERS, E. J., KIM, Y. C. & KHADRA, L. 1982 Experiments on the role of amplitude and phase modulations during the transition to turbulence. *J. Fluid Mech.* **123**, 1–29.

MOLLO-CHRISTENSEN, E. 1971 Physics of turbulence flows. *AIAA J.* **9**, 1217–1228.

MONKEWITZ, P. A. 1988 Subharmonic resonance, pairing and shredding in the mixing layer. *J. Fluid Mech.* **188**, 223–252.

MONKEWITZ, P. A. & HUERRE, P. 1982 The influence of the velocity ratio on the spatial instability of mixing layers. *Phys. Fluids* **25**, 1137–1143.

NAYFEH, A. H. 1987 On secondary instabilities in boundary layers. In *Stability of Time Dependent and Spatially Varying Flows* (ed. D. L. Dwoyer & M. Y. Hussaini), pp. 18–49. Springer.

NIKITOPOULOS, D. E. & LIU, J. T. C. 1987 Nonlinear binary–mode interactions in a developing mixing layer. *J. Fluid Mech.* **179**, 345–370.

PIERREHUMBERT, R. T. & WIDNALL, S. E. 1982 The two- and three-dimensional instabilities of a spatially periodic shear layer. *J. Fluid Mech.* **114**, 59–82.

POWERS, E. J. & MIKSAD, R. W. 1987 Polyspectral and measurements and analysis of nonlinear wave interactions. In *Nonlinear Wave Interactions in Fluids* (ed. R. W. Miksad, T. R. Akylas & T. Herbert). The Winter Annual Meeting of ASME, AMD-vol. 87, pp. 37–65.

RAETZ, G. S. 1959 A new theory of the cause of transition in fluid flows. *Norair Rep.* NOR-59-383, Hawthorne, CA.

RITZ, C. P. & POWERS, E. J. 1986 Estimation of nonlinear transfer functions for fully developed turbulence. *Physica* D **20**, 320–334.

RITZ, C. P., POWERS, E. J., MIKSAD, R. W. & SOLIS, R. S. 1988 Nonlinear spectral dynamics of a transitioning flow. *Phys. Fluids* **31**, 3577–3588.

SATO, H. 1959 Further investigation on the transition of two dimensional separated layers at subsonic speed. *J. Phys. Soc. Japan* **14**, 1797–1810.

STEGUN, G. R. & VAN ATTA, C. W. 1970 A technique for phase speed measurements in turbulent flow. *J. Fluid Mech.* **43**, 689–699.

STUART, J. T. 1960 On the nonlinear mechanisms of hydrodynamic stability. *J. Fluid Mech.* **4**, 1–21.

WINANT, C. D. & BROWAND, F. K. 1974 Vortex Pairing: the mechanism of turbulent mixing layer growth at moderate Reynolds number. *J. Fluid Mech.* **63**, 237–255.